The vertical-velocity skewness in the atmospheric boundary layer without buoyancy and Coriolis effects

The vertical-velocity skewness in the atmospheric boundary layer without buoyancy and Coriolis effects

Elia Buono,[1,2] Gabriel Katul,[1] Michael Heisel,[3] Davide Poggi,[2] Cosimo Peruzzi,[4] Davide Vettori,[2] and Costantino Manes[2]

[1)]*Department of Civil and Environmental Engineering, Duke University, Durham, North Carolina, USA*

[2)]*Dipartimento di Ingegneria dell'Ambiente, del Territorio e delle Infrastrutture, Politecnico di Torino, Torino, Italia*

[3)]*School of Civil Engineering, University of Sydney, Sydney, Australia*

[4)]*Area for Hydrology, Hydrodynamics, Hydromorphology and Freshwater Ecology (BIO-ACAS), Italian Institute for Environmental Protection and Research (ISPRA), Rome, Italy*

(*Electronic mail: elia.buono@polito.it)

(Dated: 21 October 2024)

One of the main features of near-neutral atmospheric boundary layer (ABL) turbulence is the positive vertical velocity skewness Sk_w above the roughness sublayer or the buffer region in smooth-walls. The Sk_w variations are receiving renewed interest in many climate-related parameterizations of the ABL given their significance to cloud formation and to testing sub-grid schemes for Large Eddy Simulations (LES). The vertical variations of Sk_w are explored here using wind tunnel and flume experiments collected above smooth, rough, and permeable-walls in the absence of buoyancy and Coriolis effects. These laboratory experiments form a necessary starting point to probe the canonical structure of Sk_w as they deal with a key limiting case (i.e. near-neutral conditions). Diagnostic models based on cumulant expansions, realizability constraints, and constant mass flux approach routinely employed in the convective boundary layer as well as prognostic models based on third-order budgets are used to explain variations in Sk_w for the idealized laboratory conditions. The failure of flux-gradient relations to model Sk_w from the gradients of the vertical velocity variance σ_w^2 are explained and corrections based on models of energy transport offered. Novel links between the diagnostic and prognostic models are also featured, especially for the inertial term in the third order budget of the vertical velocity fluctuation. The co-spectral properties of w'/σ_w versus w'^2/σ_w^2 are also presented for the first time to assess the dominant scales governing Sk_w in the inner and outer layers, where w' is the fluctuating vertical velocity and σ_w is the vertical velocity standard deviation.

I. INTRODUCTION

Turbulent motion is responsible for much of the transport of heat and water vapor within the planetary boundary layer[1]. This transport determines the distribution of temperature, winds, cloud formation, and precipitation[2]. For this reason, it is often stated that life on Earth as we know it would not be possible without turbulence[3]. Climate is routinely viewed as a long-term integrator of weather (measured in decades) - an assertion put forth by the Nobel laureate K. Hasselmann[4]. In Hasselmann's representation, the coupled ocean-atmosphere-cryosphere-land system is decomposed into a rapid part - the "weather" system (essentially the atmosphere) and a slowly responding "climate" system (mainly the ocean, cryosphere, and land vegetation). Weather is defined as the average state of the atmosphere determined by its temperature, atmospheric pressure, wind, humidity, precipitation, and cloud cover. Once again, averaging of these atmospheric states is required to integrate stochastic fluctuations in the aforementioned variables - and those stochastic fluctuations are traditionally attributed to turbulence. Turbulent time scales in the atmosphere span fraction of seconds (at the micro-scales) to an hour or so (for large and very large eddy motion), and it is the aggregate of these fluctuations that generate turbulent fluxes and changes in the mean state of atmospheric variables needed for simulating or modeling weather[5].

Turbulence in the atmospheric boundary layer (ABL) has a number of well-established 'signatures' in its statistics that are deemed significant for climate and meteorological modeling, dispersion studies, wind energy generation, and a plethora of other applications pertinent to atmospheric chemistry and atmospheric composition that 'feed-back' on climate[6]. The skewness of the vertical velocity component Sk_w has long been recognized as one such key feature[7] and frames the scope of this work. It is the most elementary flow statistics quantifying asymmetry due to the presence of a boundary and is given by

$$Sk_w = \frac{\overline{w'^3}}{\overline{\sigma_w^3}}, \tag{1}$$

where w' is the instantaneous vertical (or wall-normal) velocity fluctuation, overline denotes averaging over coordinates of statistical homogeneity (e.g. time averaging in many laboratory and field experiments or space-time averaging in direct numerical simulations), and $\sigma_s = (\overline{s's'})^{1/2}$ is the standard deviation or root-mean squared value of the fluctuations of any turbulent flow variable s.

In the absence of any thermal stratification or Coriolis effects, laboratory measurements of Sk_w over rough turbulent boundary layers (including k-type and d-type) suggest that $Sk_w < 0$ in the roughness sublayer (RSL) or the buffer region of smooth walls but switches to $Sk_w > 0$ in the inertial and outer-layers[8–11]. This switch was shown to be linked to a change in the type of organized eddy motion

dominating momentum transport. Sweeping motion dominates within the roughness sublayer and ejective motion in the remaining layers of the boundary layer[8,9,12]. Likewise, Sk_w over natural and artificial canopies with different densities follow similar expectations with $Sk_w < 0$ within and just above the canopy top followed by $Sk_w > 0$ for the remaining layers[9,12,13], a result consistent with other shear-driven boundary layer experiments[14]. This finding indicates that $\partial Sk_w/\partial z > 0$ for much of the boundary layer depth δ except in the buffer layer for smooth walls or roughness sublayer in rough or permeable walls, where z is the distance from the ground or zero plane displacement for canopy flows.

Moving onwards to the unstable atmospheric surface layer (ASL), early studies found that Sk_w follows expectations from Monin-Obukhov surface layer similarity theory[15], hereafter referred to as MOST, and is empirically given by[16]

$$Sk_w = C_{ASL} - \frac{0.6\xi}{1.25^3\kappa\left[(1-15\xi)^{-1/4} - 1.8\xi\right]}, \quad (2)$$

where C_{ASL} is a similarity coefficient, $\xi = z/L_o$ is the atmospheric stability parameter (for unstable atmospheric conditions, $\xi < 0$) , L_o is the Obukhov length[5], and $\kappa = 0.4$ is the von Kármán constant. These relations are consistent with the benchmark Kansas experiment that empirically demonstrated[17]

$$\frac{\kappa z}{u_*^3}\frac{\partial\overline{w'^3}}{\partial z} = -0.6\xi. \quad (3)$$

For near-neutral ASL conditions (i.e. $\xi = 0$), these experiments suggest that $Sk_w = C_{ASL} \approx 0.1$ (i.e. a positive integration constant arising from equation 3), but offer no explanation as to why. Convective boundary layers (CBLs) are also characterized by $Sk_w > 0$ over their entire depth δ[18]. In fact, experiments and Large Eddy Simulations (LES) have shown that in the CBL, $Sk_w = 0.5 - 0.6$ persists for extended regions of the CBL ($0.2 < z/\delta < 0.75$) as discussed elsewhere[19], though some LES results[20] appear to exceed field experiments in the upper regions of the CBL by a factor of two[19]. In the limit of free convection (i.e. $\xi \to -\infty$), equation 2 suggests that Sk_w=C_{ASL}+[0.6/(0.78×1.8)]=0.53, which is close to the reported $Sk_w = 0.5$ from aircraft measurements for much of the CBL[18] as well as recent measurements in the near-convective ASL[21]. Once again, such positive near-neutral Sk_w limit in the absence of stratification is not well explained.

Interest in Sk_w has been proliferating in numerous applications including non-Gaussian models for dispersion[22–25], parameterizing subgrid schemes in LES[18,26,27], delineating the fraction of time turbulent flows reside in updrafts ($w' > 0$) versus downdrafts ($w' < 0$)[28], and higher-order closure modeling of boundary layers[20,21,29]. The latter higher-order schemes are now being implemented in climate models such as the Cloud Layers Unified By Binormals (CLUBB)[30,31], among others[32]. Third-order closure schemes, especially for Sk_w, were shown to be necessary for cloud formation in different boundary layer regimes. Some studies showed that accommodating vertical velocity probability density function (PDF) asymmetry in the ABL increased low cloud fraction by 20% - 30% in stratocumulus-to-cumulus transition regions[33].

While much attention has been devoted to Sk_w within the CBL[7], less attention has been paid to models of Sk_w in near-neutral conditions, the focus here. These conditions are prevalent in many planetary flow situations (e.g. air flow over ice sheets, large open water bodies, and in many occasions over land) and form a logical limit for ABL characterizations of asymmetry, especially for vertical turbulent transport (including Sk_w). They also form limiting states for approaches such as CLUBB that must be recovered[34]. Indeed, when comparing models and LES computed Sk_w to field experiments, there is unavoidable bias regarding heterogeneity at the ground in field experiments. Heterogeneity is known to have a higher impact on variances (e.g. σ_w^2) when compared to $\overline{w'w'w'}$[18,27,35]. Thus, disagreement between LES and field experiments, even for near-neutral limits, may be due to either subgrid filtering schemes employed by the LES or simply due to the non-ideal nature of the ground surface. This attribution deficiency underscores the need for benchmark data and theories on Sk_w derived from idealized laboratory conditions at some reference stability (e.g. near-neutral), the goal here.

In the present work, we purposely distinguish between two types of models for Sk_w: diagnostic and prognostic. Diagnostic models derive relations between Sk_w (the target variable) and other statistical moments without requiring information about the physics of turbulence. They often approximate the PDF of a flow variable with cumulant expansion truncated at some order, usually third or fourth[8,9]. These diagnostic models can then be used to impose constraints such as the so-called realizability condition[29,36] first studied in the context of locally homogeneous and isotropic turbulence[37]. Prognostic models seek to predict Sk_w from lower-order moments that can be modeled from the ensemble-averaged Navier-Stokes equations (NSE) using closure schemes. One common closure scheme links $\overline{w'^3}$ to the vertical gradients of $\overline{w'w'}$ using an eddy-viscosity coefficient (K_t) given as[32,38–40]

$$\overline{w'w'w'} = -K_t\frac{\partial\overline{w'w'}}{\partial z}. \quad (4)$$

Such closure remains controversial, especially in CBL and canopy flows[20,41–43]. This motivated the development of other approaches for the CBL such as the so-called large-eddy skewed turbulence advection velocity approach or the eddy-diffusivity mass flux approach[20,29,44]. In these revisions, equation 4 is adjusted using an additive term that reflects large-scale transport commonly modeled using the aforementioned mass flux approach[44]. In such a framework, the mathematical form for w'^3 is given by[45]

$$\overline{w'w'w'} = -K_t\left[\frac{\partial\overline{w'w'}}{\partial z} - \gamma_w\right], \quad (5)$$

where γ_w is a transport term formed from a large-scale advection velocity and a characteristic time scale. In the CBL, γ_w can be related to the vertical transport of the heat flux[29,46], meaning that $\gamma_w \to 0$ as near-neutral conditions are approached. Despite these amendments, the frustration in satisfactorily closing $\overline{w'^3}$ or Sk_w remains and is captured by the statement from a leading authority in an influential article[29]

"*Certainly, the problem of parameterization of Sk_w remains. The authors should admit that they have no definitive answer at the moment*".

The two classes of models (diagnostic and prognostic) are explored herein using a unique family of data sets that include open channel flow and wind tunnel experiments over smooth walls, rough walls, and permeable walls across wide-ranging Reynolds numbers $Re_\delta = \delta u_*/\nu$ and measurement techniques, where δ is the boundary layer depth or, more in general, the outer length scale of the flow and $u_* = \sqrt{\tau_w/\rho}$ is the friction velocity based on the total or wall stress τ_w, ρ is the fluid density (air or water), and ν is the fluid kinematic viscosity. Moreover, how constraints derived from diagnostic models can be used to offer new parameterizations for prognostic models are discussed. As shall be seen, the present work leads to $\overline{w'^3}$ as

$$\overline{w'w'w'} = -\overbrace{K_t \frac{\partial \overline{w'w'}}{\partial z}}^{\text{local effects}} + \underbrace{\beta_L \overline{w'q'}}_{\text{large scale adjustment}}, \qquad (6)$$

where q' is related to the instantaneous turbulent kinetic energy, and β_L is a constant that can be derived from pressure and viscous effects on the third order budgets of $\overline{w'^3}$. In this derivation, both a local gradient-diffusion term and a non-local transport term arise from the governing equations. Moreover, the signature of the non-local or large scale effects appearing through $\overline{w'q'}$ are also confirmed through analysis of the co-spectrum between w' and w'^2 of the aforementioned laboratory studies. The experiments here will also reveal that these non-local effects are dominant over much of the boundary depth (i.e. above the roughness sublayer or the buffer region) and that they can be parameterized by a down-gradient of the turbulent kinetic energy (instead of $\partial\overline{w'^2}/\partial z$) provided an outer layer correction is accommodated in the eddy viscosity. The $\overline{w'q'}$ has already been linked through quadrant analysis and conditional sampling to the relative importance of sweeps and ejections on momentum transport[8,9]. However, those links - sometimes termed as structural models[47–49]- remain diagnostic[10,43,50]. Thus, a key novelty of the present work is a link across all the aforementioned approaches and their testing in smooth, rough, and permeable boundaries restricted to adiabatic non-rotating flows that are stationary and planar homogeneous.

II. THEORY

A. Definitions

The Cartesian coordinate system employed here sets $x = x_1$, $y = x_2$, and $z = x_3$ along the longitudinal, lateral, and vertical (wall-normal) directions, respectively, with $z = 0$ being the ground or zero-plane displacement. The instantaneous velocity components along x, y, and z directions are labeled as $u = u_1$, $v = u_2$, and $w = u_3$, respectively, with $U = \overline{u}$ defining the mean velocity. Velocity fluctuations from their time-averaged values at a point are indicated by primed quantities.

B. Diagnostic Models

The Sk_w has been linked to many flow statistics, and those links are briefly reviewed because they impose constraints on models quantifying asymmetry in w'. They also offer a compact summary of different data sets that enables comparisons across experiments.

1. Cumulant Expansion Models

The first link to be studied here is the so-called telegraph properties of the w' series and its overall intermittent behaviour. A third-order cumulant expansion of the individual probability density function (PDF) of the normalized vertical velocity $w_n = w'/\sigma_w$ is introduced and is given by[8,9,51]

$$\begin{aligned} \mathrm{PDF}(w_n) &= \mathrm{PDF_G}(w_n)\left[1 + \frac{1}{6} Sk_w \left(w_n^3 - 3w_n\right)\right], \qquad (7)\\ \mathrm{PDF_G}(w_n) &= \frac{1}{\sqrt{2\pi}} \exp\left(-\frac{w_n^2}{2}\right), \end{aligned}$$

where $\mathrm{PDF_G}(.)$ is a zero-mean unit variance Gaussian PDF and the bracketed term corrects the PDF to account for skewness only. This approximation for the PDF enables an estimate of the fraction of time w' is in an updraft (Γ_+) or downdraft (Γ_-) and is given by[10,51–53]

$$\Gamma_+ = \int_0^\infty \mathrm{PDF}(w_n) dw_n;\ \Gamma_- = \int_{-\infty}^0 \mathrm{PDF}(w_n) dw_n = 1 - \Gamma_+, \qquad (8)$$

which can be integrated using the expansion in equation 7 and arranged to yield

$$Sk_w = \sqrt{72\pi}\ (0.5 - \Gamma_+) = \sqrt{72\pi}\ (-0.5 + \Gamma_-). \qquad (9)$$

Here, updrafts and downdrafts are associated with $w' > 0$ and $w' < 0$, respectively, and no assumptions are made about turbulent stresses or heat fluxes. An $Sk_w > 0$ requires a $\Gamma_+ < 0.5$ or $\Gamma_- > 0.5$. Equation 9 is not prognostic or predictive but suggests that the mean duration of updrafts (or downdrafts) can be explained by asymmetry in the flow. As shall be seen later, links between the so-called large-eddy skewed turbulence advection velocity used in many CBL parameterizations and Γ_+ can also be established for shear-only driven flows.

Instead of updraft and downdraft, another measure that characterizes the relative importance of ejections and sweeps (i.e. ΔS_o) on momentum fluxes and linked to Sk_w can be developed using Cumulant Expansion Models (CEM) applied to the joint PDF (JPDF) of w' and u'. This measure is defined using quadrant analysis and conditional sampling and is given by[8,9]

$$\Delta S_o = \frac{\langle u'w' \rangle|_4 - \langle u'w' \rangle|_2}{\overline{u'w'}}, \qquad (10)$$

where $\langle u'w'\rangle|_i$ is a conditional average of events in quadrant i, with quadrant 2 corresponding to ejections ($u'<0, w'>0$) and quadrant 4 to sweeps ($u'>0, w'<0$). The statistic ΔS_o is the fractional difference between contributions of ejection and sweep events to the overall time-averaged flux $\overline{u'w'}$, where the sign indicates whether sweeps ($\Delta S_o>0$) or ejections ($\Delta S_o<0$) are dominant. As before, a third-order cumulant expansion of the JPDF(u', w') to link ΔS_o with key statistical moments can be developed and is given by[9]

$$\Delta S_o = \frac{M_{11}+1}{M_{11}\sqrt{2\pi}}\left[\frac{2C_1}{(1+M_{11})^2}+\frac{C_2}{1+M_{11}}\right], \tag{11}$$

where C_1 and C_2 are defined as

$$C_1 = \left(1+M_{11}\right)\left[\frac{1}{6}(M_{03}-M_{30})+\frac{1}{2}(M_{21}-M_{12})\right]$$
$$C_2 = -\left[\frac{1}{6}(2-M_{11})(M_{03}-M_{30})+\frac{1}{2}(M_{21}-M_{12})\right], \tag{12}$$

and the so-called 'M' notation (i.e. M_{ij}) is used to describe different statistical (mixed) moments of u' and w' as

$$M_{ij} = \frac{\overline{u'^i w'^j}}{\sigma_u^i \sigma_w^j}. \tag{13}$$

In M notation, M_{11} defines the correlation coefficient $\overline{w'u'}/(\sigma_u\sigma_w)$, $M_{30}=Sk_u$ and $M_{03}=Sk_w$ define individual skewness values for u' and w', respectively, and M_{12} (associated with wall-normal turbulent transport of flux) and M_{21} (associated with wall-normal turbulent transport of longitudinal velocity variance) define third-order mixed moments. When equation 12 is inserted into equation 11, the final form linking ΔS_o to the statistical moments is

$$\Delta S_o = \frac{1}{M_{11}2\sqrt{2\pi}}\left[\frac{M_{11}}{3}(M_{03}-M_{30})+(M_{21}-M_{12})\right]. \tag{14}$$

A large corpus of experiments on momentum transport over smooth surfaces and differing types of roughness elements suggest a linear relation between each of the third-order moments. Specifically, $M_{30}=b_u M_{12}$, $M_{03}=b_w M_{12}$, and $M_{21}=b_{uw}M_{12}$ where the respective constant values $b_u\approx 2$, $b_w\approx -1.16$, and $b_{uw}\approx -1$ were presented elsewhere[9,10]. The value $b_{uw}\approx -0.6$ was also reported for flows within and just above dense canopies across a wide range of thermal stratification conditions[50,52,54]. Inserting these linear relations into equation 14 and simplifying yields[10]

$$Sk_w = M_{03} \approx \frac{2b_w\sqrt{2\pi}}{\frac{1}{3}M_{11}(b_w-b_u)+(b_{uw}-1)}M_{11}\Delta S_o. \tag{15}$$

In dimensional form, the sought link between $\overline{w'w'w'}$ and $\sigma_w^3\Delta So$ is now given by

$$\overline{w'w'w'} \approx \frac{2b_w\sqrt{2\pi}}{\frac{1}{3}M_{11}(b_w-b_u)+(b_{uw}-1)}\sigma_w^3 M_{11}\Delta S_o. \tag{16}$$

This relation reveals a $\overline{w'w'w'}$ that is not proportional to $\partial\sigma_w^2/\partial z$ as modeled by gradient-diffusion arguments[38] such as the one in equation 4 in the absence of large scale adjustment. Equating this outcome to equation 9 yields an interesting connection between Γ_+ and ΔS_o given by

$$\frac{2b_w}{\frac{1}{3}M_{11}(b_w-b_u)+(b_{uw}-1)} = 6\,C_{CEM}; \qquad C_{CEM}M_{11}\Delta S_o = 0.5-\Gamma_+. \tag{17}$$

Here, C_{CEM} is a coefficient that is not constant and varies with z due to the z-variations in M_{11}. The latter result is suggestive of a connection between the time fraction in updrafts and downdrafts and the stress fractional imbalance between ejections and sweeps. When $Sk_w>0$, $0.5-\Gamma_+>0$, ejections occur less than 50% of the time yet equation 17 adds an extra finding that ejections dominate momentum transport over sweeps (i.e. $\Delta S_o<0$).

2. Realizability Constraints

One class of models propose that deviations from Gaussian distribution must impact Sk_w as well as the flatness factor $FF_w=\overline{w'^4}/\sigma_w^4$ with some coordination. The 'essence' of this argument is that the mechanisms that generate asymmetry (e.g. Sk_w) are not entirely independent of the mechanisms that produce large-scale intermittency (e.g. FF_w). Realizability constraints have been used to guide the development of such coordination between Sk_w and FF_w, especially in the CBL. In more detail, two random variables $a'=w'$ and $b'=w'w'$ must satisfy the statistical constraint

$$\overline{a'b'} \le \sigma_a\sigma_b, \tag{18}$$

where $\sigma_a=\sigma_w$ and $\sigma_b=\sigma_{w^2}=\left[\overline{(b'-\overline{b'})^2}\right]^{1/2}=\left[\overline{(w'^2-\overline{w'^2})^2}\right]^{1/2}$. Expanding this expression yields

$$\sigma_{w^2} = \left(\overline{w'^4}-(\overline{w'^2})^2\right)^{1/2} = \left[FF_w\sigma_w^4-(\sigma_w^2)^2\right]^{1/2} = \sigma_w^2(FF_w-1)^{1/2}. \tag{19}$$

Inserting this finding into equation 18 and re-arranging results in

$$\overline{w'w'w'} \le \sigma_w^3(FF_w-1)^{1/2}. \tag{20}$$

Upon dividing both sides by σ_w^3 and squaring yields $Sk_w^2 \le FF_w-1$. When these inequality constraints are written as equalities with unknown coefficient, they can be expressed as[36,55]

$$FF_w = \alpha_1(Sk_w^2+1), \tag{21}$$

where α_1 is a model parameter that should exceed unity to ensure realizability. For a Gaussian PDF, the $Sk_w=0$, $FF_w=3$, and $\alpha_1=3$ (>1). Empirical values ranging from $2.6-3.3$ have been reported across a number of field experiments and LES[14,55]. This class of models will also be considered using the data here - as it facilitates a new closure scheme for the budgets of w'^3 to be derived later on in the prognostic models section.

3. The Fractional Area/Mass Flux Approach

The Sk_w can also be used to define a so-called turbulent advection velocity w_a using

$$w_a = \frac{\overline{w'^3}}{\sigma_w^2} = Sk_w\sigma_w, \tag{22}$$

and this advection velocity is employed to parameterize top-down and bottom-up diffusion in CBLs[29]. In the eddy advection velocity model, the fractional area occupied by updrafts (w_+) and downdrafts (w_-) are a and $1-a$. These fractional areas are presumed constant, which may be plausible in the CBL but not necessarily in the near-neutral ABL (to be explored here). Nevertheless, it is instructive to ask what such a model predicts for Sk_w. For a constant a[44], the conservation of fluid mass leads to the following expressions for the large eddy skewed advection velocity approach:

$$aw_+ + (1-a)w_- = 0, \tag{23}$$
$$aw_+^2 + (1-a)w_-^2 = \sigma_w^2, \tag{24}$$
$$aw_+^3 + (1-a)w_-^3 = (Sk_w)\sigma_w^3, \tag{25}$$
$$aw_+^4 + (1-a)w_-^4 = (FF_w)\sigma_w^4. \tag{26}$$

These expressions describe the first four moments and can be solved to yield

$$\begin{aligned} w_+ &= -\frac{1-a}{a}w_-, \text{ and } w_- = \pm\frac{\sigma_w}{\sqrt{(1/a)-1}}, \\ a &= \frac{1}{2} \pm \frac{Sk_w}{2\sqrt{4+Sk_w^2}}, \text{ or } Sk_w^2 = -4 + \frac{1}{a} + \frac{1}{1-a}, \\ FF_w &= -3 + \frac{1}{a(1-a)}, \text{ or } FF_w = 1 + Sk_w^2. \end{aligned} \tag{27}$$

This latter finding is identical to equation 21 when setting $\alpha_1 = 1$, which is the minimum α_1 necessary for satisfying the realizability constraint as shown in equation 20. When equating equation 9 to the outcome of equation 27, a relation between a (fractional area contribution by updrafts) and Γ_+ (time fraction of updrafts) can be established, i.e.

$$a = \frac{1}{2} \pm \frac{1}{2}\frac{\sqrt{72\pi}(0.5-\Gamma_+)}{\sqrt{4+72\pi(0.5-\Gamma_+)^2}}. \tag{28}$$

While a (a spatial quantity) is not linearly related to Γ_+, a one-to-one correspondence has been established here. On a similar note, variants on this approach replace a and $1-a$ with PDF($w' > 0$) and PDF($w' < 0$) as discussed elsewhere[29].

C. Prognostic Models

These models are based on moment expansion of the NSE and closure schemes that link higher- to lower order moments. The prognostic approach commences with the governing equation for w. The first, second, and third order budgets for the statistics of w' are reviewed here along with conventional closure models employed. Proposed revisions to them, especially for the third order budgets are also presented. For an incompressible or constant density flow, the instantaneous equation for w (or w') in the absence of stratification and Coriolis is given by

$$\frac{\partial w}{\partial t} + u\frac{\partial w}{\partial x} + v\frac{\partial w}{\partial y} + w\frac{\partial w}{\partial z} = -\frac{1}{\overline{\rho}}\frac{\partial P}{\partial z} - g + \nu\frac{\partial^2 w}{\partial x_j \partial x_j}, \tag{29}$$

where t is time, ρ is the fluid density (constant here), P is the pressure, and the repeated i index denotes summation over spatial coordinates ($[x_1, x_2, x_3] = [x, y, z]$).

1. First Moment

Upon expressing the left-hand side of equation 29 in a mass-preserving form

$$\frac{\partial w}{\partial t} + \frac{\partial (uw)}{\partial x} + \frac{\partial (vw)}{\partial y} + \frac{\partial (ww)}{\partial z} = \cdots, \tag{30}$$

then averaging while assuming stationary (i.e. $\partial\overline{(.)}/\partial t = 0$) and planar homogeneous (i.e. $\partial\overline{(.)}/\partial x_1 = \partial\overline{(.)}/\partial x_2 = 0$) flow in the absence of subsidence (i.e. $\overline{w} = 0$), the vertical velocity variance budget can be derived and is given by

$$\overbrace{\frac{\partial \overline{w'w'}}{\partial z}}^{\text{Inertial Term}} = \underbrace{-\frac{1}{\overline{\rho}}\frac{\partial \overline{P}}{\partial z}}_{\text{Pressure Gradient}} \overbrace{-g}^{\text{Gravitational Acceleration}}, \tag{31}$$

which upon integration with respect to z yields a Bernoulli-like equation

$$\overline{w'w'} + \frac{\overline{P}}{\overline{\rho}} + gz = C_B, \tag{32}$$

where C_B is a constant of integration. When $\overline{P} = -\overline{\rho}gz$ (i.e. hydrostatic approximation), $\partial\sigma_w^2/\partial z = 0$ or σ_w must be a constant $= \sqrt{C_B}$ and independent of z. Thus, deviations from a constant σ_w^2 in z signifies deviations from hydro-static assumption in the mean pressure vertical gradient.

2. Second Moment

The budget equation for $\overline{w'w'}$ can be similarly derived by multiplying equation 29 by $2w'$ and averaging to yield

$$\overbrace{\frac{\partial \overline{w'w'w'}}{\partial z}}^{\text{Inertial Term}} = \underbrace{-\frac{2}{\overline{\rho}}\overline{w'\frac{\partial p'}{\partial z}}}_{\text{Pressure}-\text{Velocity Interaction}} + 2\underbrace{\nu\overline{w'\frac{\partial^2 w'}{\partial x_i \partial x_i}}}_{\text{Viscous Destruction}}, \tag{33}$$

where p' is turbulent pressure deviation from the mean or hydrostatic state. This budget identifies two mechanisms that

impact $\partial\overline{w'^3}/\partial z$: The first is a pressure-velocity interaction term that can act as a source or a sink as later discussed and the second is a viscous destruction term that acts as a sink term. A model for the pressure-velocity interaction term is needed to mechanistically link the skewness to turbulent processes. This term may be modeled using a linear return-to-isotropy Rotta scheme[56] modified here to maintain the pressure transport term[46]. It is given by[46,56,57]

$$-2\overline{w'\frac{\partial p'}{\partial z}} = \frac{C_R}{\tau}\left(\frac{2K}{3} - \overline{w'^2}\right) - 2\frac{\partial}{\partial z}\overline{w'p'}, \tag{34}$$

where τ is a time scale, $C_R = 1.8$ is the Rotta constant, $K = (1/2)\overline{u_i'u_i'}$ is the turbulent kinetic energy at z. The Rotta model actually applies to $\overline{p'\partial w'/\partial z}$ (i.e. no gradients in p' emerge). However, $\partial(\overline{w'p'})/\partial z = \overline{p'\partial w'/\partial z} + \overline{w'\partial p'/\partial z}$, which is why the pressure transport term emerges in equation 34. The term $\partial(\overline{w'p'})/\partial z$ has been ignored in many atmospheric turbulence studies[5,7] but can be included if finite and known[58].

At large scales, the redistribution of kinetic energy among velocity components by the pressure term to achieve an equipartition state is reasonably established[59–61]. Because the viscous dissipation rate of K ($= \varepsilon > 0$) occurs at small (or micro) scales that are presumed to be isotropic, it is reasonable to assume that $\varepsilon_u = \varepsilon_v = \varepsilon_w = (1/3)\varepsilon$, where ε_u, ε_v, ε_w are the viscous dissipation rates of $\overline{u'u'}$, $\overline{v'v'}$, and $\overline{w'w'}$. Thus, with a return to isotropy closure and an isotropy of dissipation rate of K, a model for $\overline{w'^3}$ may be constructed and is given as[57]

$$\frac{\partial\overline{w'w'w'}}{\partial z} = \frac{C_R}{\tau}\left(\frac{2K}{3} - \overline{w'^2}\right) - \frac{1}{3}\varepsilon. \tag{35}$$

In the original Rotta scheme, $\tau = 2K/\varepsilon$ (i.e. return-to-isotropy time scale is proportional to the relaxation time scale via C_R) and equation 35 can be expressed in non-dimensional form as

$$\frac{1}{\varepsilon}\frac{\partial\overline{w'w'w'}}{\partial z} = C_R\left(\frac{1}{3} - \frac{\overline{w'^2}}{2K}\right) - \frac{1}{3}. \tag{36}$$

It is instructive to inquire about a reference state that result in a zero vertical gradient in $\overline{w'^3}$ similar to the analysis leading to a constant σ_w^2 with z variations. From the analysis above, this state is achieved when the anisotropy measure $A_w = \sigma_w^2/(2K)$ is a constant given by an equilibrium value

$$A_{w,e} = \frac{1}{3} - \frac{1}{3C_R}. \tag{37}$$

For a $C_R = 1.8$ (or a $C_R = 0.9$ when K is used in lieu of $2K$), $A_{w,e} = 0.15$. In the inertial sublayer (ISL) of the atmosphere (or near-neutral ASL), common values for the second moments are $\sigma_u/u_* = 2.4$, $\sigma_v/u_* = 2.1$, and $\sigma_w/u_* = 1.25$ so that typical ISL values for $A_w = 0.13$, close to the predicted value ($= 0.15$) from C_R only. Thus, it is expected that $\overline{w'^3}$ be a constant independent of z as these idealized conditions are approached. Equation 36 makes clear that a reduction in A_w below $A_{w,e}$ leads to $\partial\overline{w'^3}/\partial z > 0$. In general, wall-blocking in the RSL and contributions from large eddies to K in the outer layer tend to reduce A_w below $A_{w,e}$. Thus, in both regions, $\partial\overline{w'^3}/\partial z > 0$.

For completeness, deviations from small-scale isotropy (i.e.ε_u=ε_v=ε_w) can be accommodated in this framework as these conditions may occur when the Reynolds numbers are not high. If small-scale anisotropy does persist[62], then it is convenient to express $\varepsilon_u + \varepsilon_v = \alpha_d\varepsilon_w$, where $\alpha_d < 2$ as discussed elsewhere[57]. For such anisotropy, $\varepsilon_w = \varepsilon/(1+\alpha_d)$ and

$$\frac{1}{\varepsilon}\frac{\partial\overline{w'w'w'}}{\partial z} = C_R\left(\frac{1}{3} - \frac{\overline{w'^2}}{q^2}\right) - \frac{1}{1+\alpha_d}. \tag{38}$$

This implies that $A_{w,e}$ must be modified to $A_{w,ani}$ so as to include small-scale anisotropy in the turbulent kinetic energy dissipation rates. These corrections are not pursued further given the uncertainty in the dissipation rate estimates in the data sets used here.

3. Third Moment

The budget for the time rate of change of $\overline{w'w'w'}$ can be derived by multiplying equation 29 with $3w'^2$ and averaging the outcome to yield[46,63,64]

$$\frac{\partial\overline{w'^3}}{\partial t} = 0 = \overbrace{-\frac{\partial\overline{w'w'^3}}{\partial z} + 3\overline{w'w'}\frac{\partial\overline{w'w'}}{\partial z}}^{\text{Inertial Term}} \underbrace{-\frac{3}{\overline{\rho}}\left(\overline{w'w'\frac{\partial p'}{\partial z}}\right)}_{\text{Pressure}-\text{Velocity Interaction}} \underbrace{-2\nu\left(\overline{3w'\frac{\partial w'}{\partial x_i}\frac{\partial w'}{\partial x_i}}\right)}_{\text{Viscous Destruction}}. \tag{39}$$

To close the fourth moment, a number of possibilities exist. To maintain generality, the inertial term can be formulated as

$$-\frac{\partial\overline{w'^4}}{\partial z} + 3\overline{w'w'}\frac{\partial\overline{w'w'}}{\partial z} = -\sigma_w^4\frac{\partial FF_w}{\partial z} + \sigma_w^2(3 - 2FF_w)\frac{\partial\sigma_w^2}{\partial z}. \tag{40}$$

The most common closure is the quasi-Gaussian approximation setting $FF_w = 3$ without making any assumptions about the asymmetry[36]. In this case, $\partial FF_w/\partial z = 0$ and the inertial term reduces to $-3\sigma_w^2(\partial\sigma_w^2/\partial z)$. Another option is to use the result of equation 21. As simplification, it is assumed that the first term on the right-hand side of equation 40 is much smaller than the second term so that:

$$-\frac{\partial\overline{w'^4}}{\partial z} + 3\sigma_w^2\frac{\partial\sigma_w^2}{\partial z} = \sigma_w^2\left[3 - 2\alpha_1\left(Sk_w^2 + 1\right)\right]\frac{\partial\sigma_w^2}{\partial z}. \tag{41}$$

Interestingly, when $Sk_w^2 << 1$, and α_1 does not deviate appreciably from 3, the Gaussian approximation is recovered. Thus, the closure in equation 41 suggests that some deviations from Gaussian can be accommodated provided FF_w does not vary appreciably with z.

Closure models for the pressure-velocity interaction and viscous dissipation terms have been proposed[46,63,64]. A linear return to isotropy scheme yields[56]

$$-\frac{3}{\overline{\rho}}\left(\overline{w'w'\frac{\partial p'}{\partial z}}\right)=\frac{3}{2}\frac{C_R}{\tau_s}\left(\frac{\overline{w'q'}}{3}-\overline{w'w'^2}\right), \tag{42}$$

and the viscous dissipation contribution can be modeled as

$$2\nu\left(3\overline{w'\frac{\partial w'}{\partial x_i}\frac{\partial w'}{\partial x_i}}\right)=2\overline{\varepsilon' w'}=c_2\frac{\overline{w'q'}}{\tau_s}, \tag{43}$$

where c_2 is a similarity constant, $q'=u_i'u_i'$, ε' is the fluctuating dissipation rate, and τ_s is a decorrelation time scale that need not be identical to τ because w' and the instantaneous time scale ε'/q' can be correlated. Here, the interaction between w' and the pressure transport term has been ignored though its effect can be accommodated if necessary.

Inserting these approximations into equation 39 yields[64],

$$\overline{w'^3}=\overbrace{-\frac{2\tau_s\sigma_w^2}{3C_R}\frac{\partial\overline{w'w'}}{\partial z}}^{\text{Gradient}-\text{Diffusion}}+\overbrace{\overline{w'q'}\left(\frac{1}{3}-\frac{2c_2}{3C_R}\right)}^{\text{Non}-\text{local Transport}}. \tag{44}$$

For operational purposes, a model for $\overline{w'q'}$ is needed to prognostically determine Sk_w. A plausible closure that has been extensively studied is[64,65]

$$\overline{w'q'}=-\kappa z u_*\phi_L(z)\frac{\partial(2K)}{\partial z}, \tag{45}$$

where ϕ_L is a correction to accommodate outer layer effects[66]. It is common in open channel flows to assume $\phi_L(z)=1-z/\delta$. In atmospheric boundary layers and wind tunnels, $\phi_L(z)=(0.5+\kappa z/\alpha_m\delta)^{-1}$, where $\alpha_m=\kappa/4$. The quadratic variation in z of the eddy diffusivity has been proposed in earlier modeling studies of momentum transfer[67] and tested for open channel flows[65]. For $z/\delta<<0.1$, the eddy diffusivity increases linearly with z. However, the quadratic term in z becomes the dominant term as z/δ increases beyond 0.5. For wind tunnels, ϕ_L increases monotonically and approaches a constant (and maximum) value. Inserting this closure into equation 44 yields[64]

$$Sk_w=-\frac{2}{3C_R}\left[A_{t,w}\frac{\partial\overline{w'w'}}{\partial z}+B_{t,u}\frac{\partial K}{\partial z}\right], \tag{46}$$

where

$$A_{t,w}=\frac{\tau_s}{\sigma_w};B_{t,u}=(C_R-2c_2)\frac{\kappa z u_*\phi_L(z)}{\sigma_w^3}. \tag{47}$$

Because $K=(1/2)(\sigma_u^2+\sigma_v^2+\sigma_w^2)$ and $\sigma_u^2\approx\sigma_v^2+\sigma_w^2$, it follows that $K\approx\sigma_u^2$ and $\partial K/\partial z$ can be replaced by $\partial\sigma_u^2/\partial z$. It is worth noting that, even within a near-neutral ASL, σ_u is impacted by eddies much larger than z consistent with Townsend's attached eddy model[64,68–70]. A plausible choice is $\tau_s=\kappa z u_*\phi_L(z)/u_*^2$, which makes the two eddy viscosity formulations for $A_{t,w}$ and $B_{t,u}$ comparable in magnitude in the ISL and outer layer, as routinely done in turbulence closure schemes.

III. DATA SETS

The data sets have been collected over smooth walls[71–73], rough walls[10], and permeable walls with varying permeability and Reynolds numbers[71]. Table I summarizes the experimental conditions and the data sets as well as the original sources describing the experiments. Data sets came from both open channel flows (OC) and wind tunnel (WT) experiments. Longitudinal and wall normal flow velocities have been measured with laser doppler anemometry in OC and with cross-hotwire anemometry in WT experiments. Permeable wall experiments have been performed with bed porosity measured in pores per inches (ppi) of 60 (MNP1, MNP2), 30 (MNP3, MNP4) and 10 (MNP5). Rough wall experiments (HLR1, HLR2) have been performed with a woven wire mesh with a roughness length of 6 mm. More methodological details are provided in the original sources presented in Table I. These data sets represent canonical wall-bounded flows and lack certain complexities that are present in the ABL even under neutral conditions and in the absence of Coriolis effects. The chief complexity absent here is the effect of a stratified capping inversion that influences the outer region behavior of the conventionally neutral ABL. This effect is likely to modify, at minimum, the $\phi_L(z)$ formulation.

IV. RESULTS

The results section investigates the diagnostic models first and then proceeds to explore the prognostic model predictions using the third order budget. Agreement between model predictions and experiments is evaluated using linear regression analysis where the coefficient of determination (R^2) is presented on Figures 3, 6, 9a and 11. Before doing so, the measured first and second moments are reported and discussed in Figure 1 for completeness. The normalized mean velocity as a function of z/δ (i.e. presented with outer layer variables) shows large differences across experiments due to simultaneous Reynolds number and roughness effects. No expected collapse of the data onto a single curve is expected when using such outer scaling variables for U/u_* (Figure 1a). Much of the scatter in the second moments is deemed to be below the inertial sublayer (ISL) - roughly below $z/\delta=0.1$ (Figure 1b-d). Data below this limit have been neglected for statistical validation of the proposed models (i.e. coefficient of determination, R^2). A region of constant stress and constant σ_w^2 exists for $z/\delta\in[0.08,0.2]$ across most of the data sets (Figure 1b). This region delineates operationally the ISL. For $z/\delta>0.3$, the σ_w^2/u_*^2, σ_u^2/u_*^2, and $\overline{u'w'}/u_*^2$ decline in magnitude with increasing z/δ, which is of significance to prognostic models explaining the sign of Sk_w and the dominant processes controlling its magnitude.

A. Cumulant Expansion Models

Figure 2 presents the measured values of Γ_+, ΔS_o, and a as a function of z/δ. For $z/\delta>0.08$, all data sets suggest

TABLE I. Summary of the data sets used in the analysis. Bed types are classified as S smooth, P porous, and R rough. Flow types are reported as OC for open channels, and WT for wind tunnels. For convenience, the symbols used in the figures are reported here as well.

Source	Data set	Bed	Flow	$\delta \times 10^{-3}[m]$	$u_* \times 10^{-3}[m/s]$	Re_τ	Symbol
Manes, Poggi, and Ridolfi [71]	MNS	S	OC	60	41	2160	○
	MNP1	P	OC	96	28	2349	+
	MNP2	P	OC	110	34	3234	✳
	MNP3	P	OC	115	18	1856	·
	MNP4	P	OC	146	46	5840	×
	MNP5	P	OC	89	49	3848	□
Heisel *et al.* [10]	HLR1	R	WT	408	370	9611	◇
	HLR2	R	WT	391	550	13683	△
	HLS1	S	WT	222	260	3681	▽
	HLS2	S	WT	203	350	4536	▷
Peruzzi *et al.* [72]	PRS1	S	OC	200	10	1730	◁
	PRS2	S	OC	120	8	795	☆
	PRS3	S	OC	85	22	1657	✡
Poggi, Porporato, and Ridolfi [73]	PGS1	S	OC	50	21	1071	−
	PGS2	S	OC	45	7	331	∣
	PGS3	S	OC	42	30	1232	+
	PGS4	S	OC	46	19	845	✳

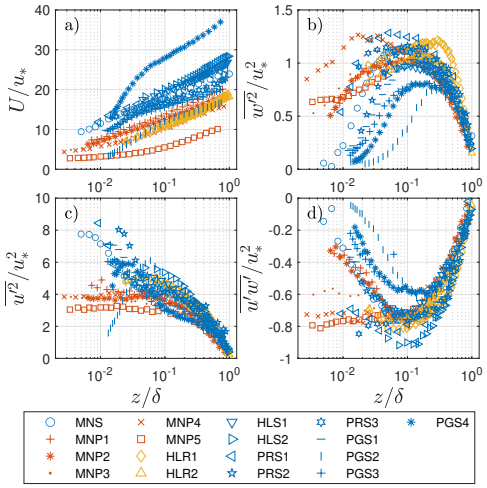

FIG. 1. Measured values of: (a) normalized mean velocity U/u_*, (b) vertical velocity variance $\overline{w'^2}/u_*^2$, (c) longitudinal velocity variance $\overline{u'^2}/u_*^2$, and (d) turbulent stress $\overline{u'w'}/u_*^2$ as a function of the normalized wall normal distance z/δ. In this and all later figures, the symbols correspond to the data sets in Table I.

$0.5-\Gamma_+ > 0$. In fact, for $z/\delta \in [0.1, 0.3]$, $0.48 < \Gamma_+ < 0.50$ for all datasets except one (PGS2 with Re_τ=331), which is approximately constant with respect to z variations. The collapse of the data sets for ΔS_o is also rather remarkable when inspecting the same interval $z/\delta \in [0.1, 0.3]$. For $z/\delta > 0.07$, all data sets suggest ejections dominate ($\Delta S_o < 0$) consistent with rough-wall wind tunnel[9] and smooth-wall open channel flow[8] experiments. As $z/\delta > 0.9$, ΔS_o becomes ill-defined because the turbulent stress is small. Last, it is noted that the predicted a appears independent of z for $z/\delta \in [0.1, 0.3]$, while it is substantially reduced when $z/\delta > 0.3$ for the majority of datasets. However, the most consistent behaviour in terms of 'data collapse' identifying the strength of ejections across datasets appears to be ΔS_o (as expected).

The relation between measured Sk_w and predictions from Γ_+ using equation 9 (i.e. using CEM) is shown in Figure 3. The agreement is acceptable considering that this comparison covers all sublayers including the buffer- and roughness-sublayers. As predicted by equation 9, when $0.5-\Gamma_+ > 0$, the $Sk_w > 0$, and conversely. Likewise, the ratio of ΔS_o modeled using a third order CEM applied to the JPDF(w', u') to measured ΔS_o as a function of z/δ is also shown in Figure 4. Once again, the agreement is acceptable for much of the boundary layer region ($z/\delta \in [0.1, 0.9]$). The values of the individual moments M_{ij} used in the determination of $\Delta S_{o,m}$ (modeled using CEM) as a function of z/δ are presented in Figure 5. The most consistent collapse across all data sets is for $M_{03} = Sk_w$ in the region of $0.1 < z/\delta < 0.9$ (Figure 5b) followed by M_{12} (Figure 5d). Moreover, there is a notable collapse of $M_{03} = Sk_w$ to a near-constant positive value for $z/\delta \in [0.08, 0.3]$, namely in the ISL, consistent with previous empirical studies[16]. The height independence of M_{12} was proposed to delineate the ISL in some studies on rough-wall turbulence[65] though it appears from the analysis here that M_{03} may be an acceptable single-variable substitute. Across all data sets and regions, the $C_{CEM}M_{11}\Delta S_o$ appears to vary linearly with $0.5-\Gamma_+$ as shown in Figure 6. This linearity is consistent with predictions from equation 14 and suggests that Sk_w, Γ_+, and $C_{CEM}M_{11}\Delta S_o$ are linearly related as foreshadowed from third order CEMs (see equation 17). A main finding is that Γ_+ contains significant information about imbalances between sweeps and ejections responsible for momentum transfer.

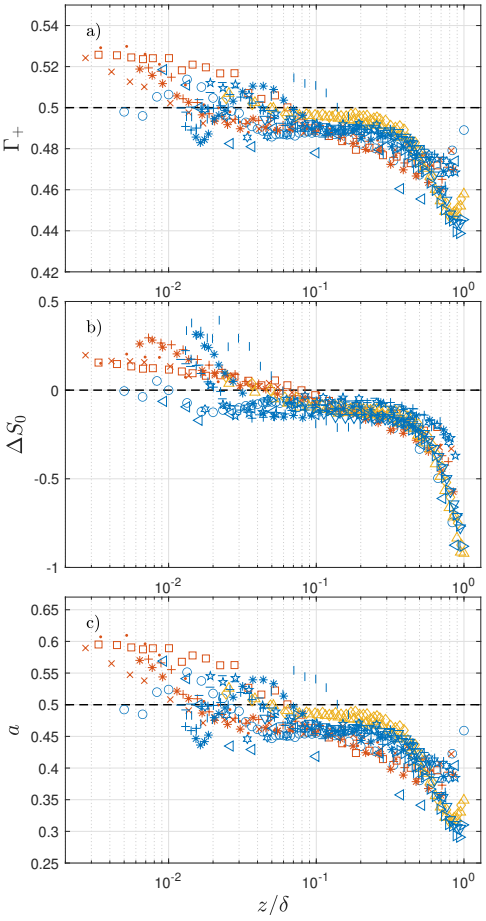

FIG. 2. Measured values of: (a) the fraction of time $w' > 0$ (or Γ_+), (b) the imbalance between sweeps and ejection contributions to the Reynolds stress (or ΔS_o), and (c) the fractional area a of updrafts as a function of the normalized wall normal distance z/δ. The horizontal dashed lines indicate the conditions whereby updrafts and downdrafts are perfectly balanced.

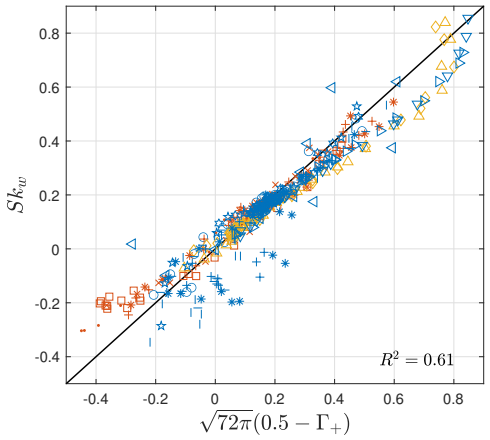

FIG. 3. Comparison between vertical velocity skewness (Sk_w) modeled using third-order cumulant expansion (via measured Γ_+) and measured Sk_w. All values of z/δ are included.

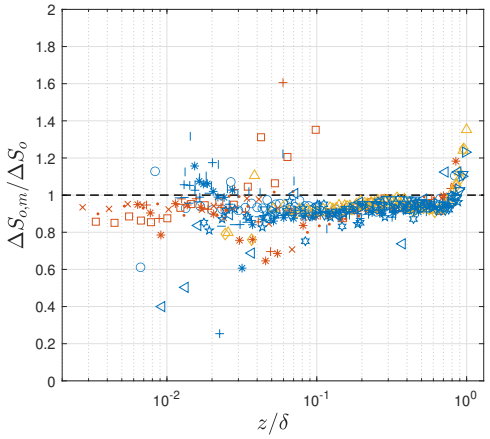

FIG. 4. Ratio of $\Delta S_{o,m}$ modeled using the third-order cumulant expansion and measured ΔS_o (computed from quadrant analysis) as a function of z/δ.

B. Realizability Constraints

In general, the skewness and flatness factors of a PDF are independent quantities. However, in turbulence modeling the nature of the second-order non-linearity of the Navier-Stokes equation means that budgets for the statistical moment m of a single flow variable such as w', require moment $m+1$ to be known. Therefore, it may be conjectured that the physics of turbulence requires some coordination between FF_w and Sk_w. The realizability constraint as formulated here links Sk_w to FF_w by replacing inequalities with equalities along with associated coefficients such as α_1. It is important to note that this inequality constraint is only statistical (i.e. applies to any random variable) and replacing inequalities with equalities is not derived from the physics of turbulence. Nonetheless, Figure 7c shows the variations in α_1 using measured Sk_w and FF_w as a function of z/δ (reported in Figure 7a-b). For $0.07 < z/\delta < 0.9$, the values of α_1 are around 3.3 for all data sets. This finding supports the working assumption that the inertial term in the third-order budget of $\overline{w'^3}$ reduce

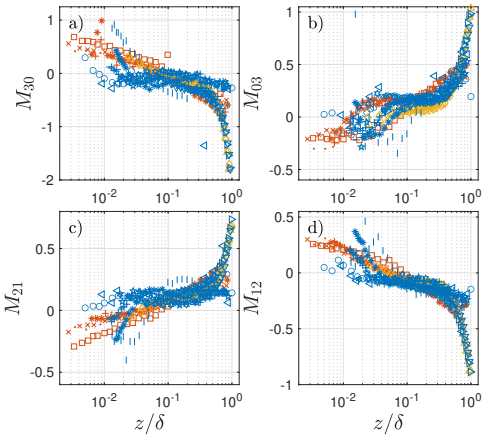

FIG. 5. The variations of the triple moments: (a) M_{30} skewness of u', (b) M_{03} skewness of w', (c) M_{21} mixed moment of u'^2 and w' and (d) M_{12} mixed moment of u' and w'^2, as a function of the normalized wall normal distance z/δ.

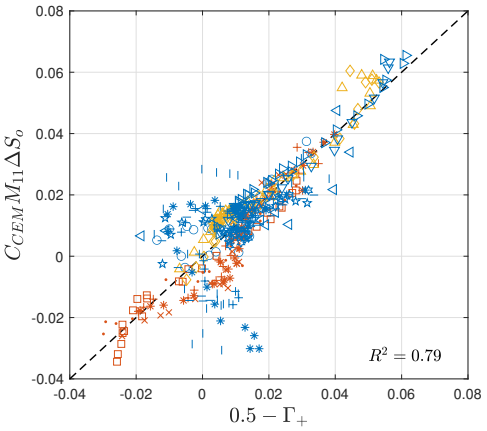

FIG. 6. Comparison between $0.5-\Gamma_+$ and measured $C_{CEM}M_{11}\Delta S_o$. The one-to-one line is based on the simplified CEM representation used to obtain equation 17.

to $(3-2\alpha_1)\sigma_w^2(\partial\sigma_w^2/\partial z)$. Moreover, an $\alpha_1 = 3.3$ is sufficiently close to a Gaussian value when modeling the entire inertial term using a Gaussian approximation (i.e. $\alpha_1 = 3$) and deviates appreciably from the prediction by the fractional area/mass flux approach that leads to $\alpha_1 = 1$.

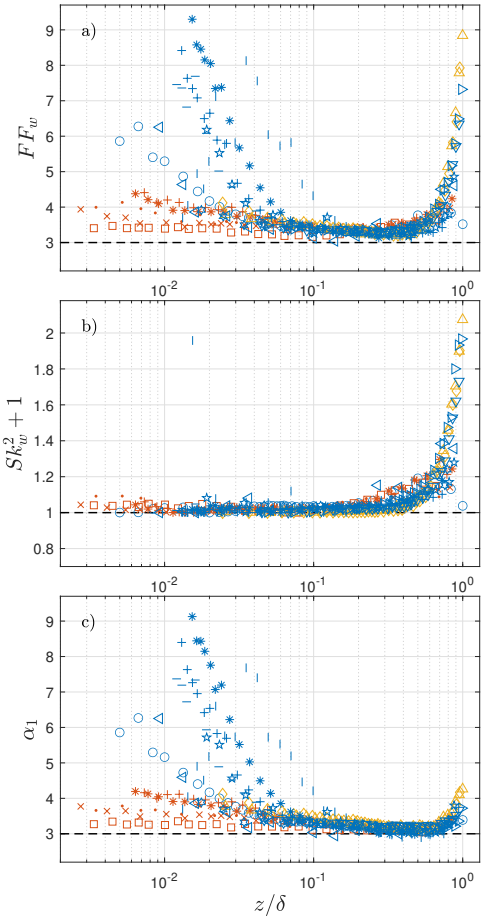

FIG. 7. The variations of: (a) measured FF_w, (b) measured Sk_w^2+1, and (c) α_1 estimated from FF_w and Sk_w^2+1 as a function of the normalized wall normal distance z/δ. The horizontal dashed lines indicate the Gaussian approximation.

C. Gradient-Diffusion Prognostic Models

Equation 4 is used to compute the eddy diffusivity K_t by dividing measured $\overline{w'^3}$ with measured $\partial\sigma_w^2/\partial z$. The K_t thus estimated is then normalized using $\sigma_w^2\kappa z/u_*$ to be consistent with prior studies[65]. The outcome is shown in Figure 8: for $0.3 < z/\delta < 0.9$, K_t decays with increasing z/δ; for $z/\delta < 0.3$, which includes the ISL, the approach spectacularly fails even at predicting the sign of K_t. More interesting is that this failure may be decomposed into two regions: (i) a finite Sk_w associated with a zero vertical velocity variance gradient roughly in

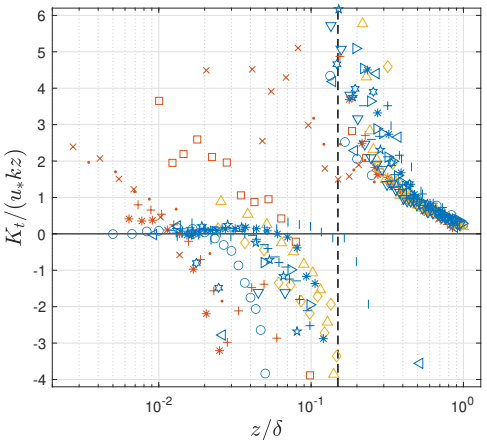

FIG. 8. The variation of the normalized computed eddy diffusivity K_t as a function of the normalized wall normal distance z/δ. The vertical dashed line roughly indicates $\partial\sigma_w^2/\partial z = 0$. The horizontal line is $K_t = 0$.

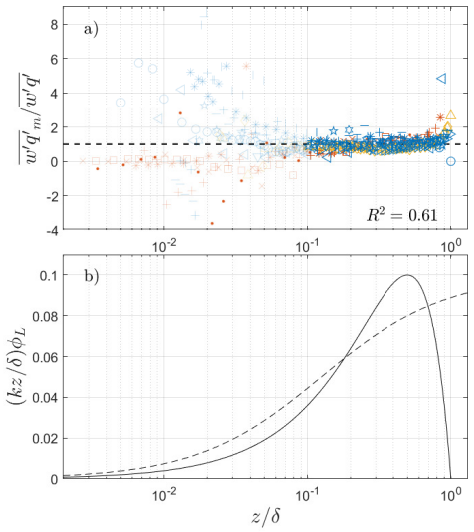

FIG. 9. (a) Comparison between measured and down-gradient modeled vertical transport of turbulent kinetic energy when setting $q_m = u'^2$. The shaded markers indicate $z/\delta < 0.1$. The horizontal dashed line denotes a perfect agreement between model and data. (b) The assumed effective dimensionless mixing length $\kappa(z/\delta)\phi_L(z/\delta)$ for open channel flows (solid line) and wind tunnels (dashed line). Note the parabolic behavior for open channel flows (characterised by a free surface) and the monotonically increasing values for wind tunnel studies.

the ISL, and (ii) an unphysical negative diffusivity, mainly in the buffer region or roughness sublayer depending on the data set. The cross-over occurs when $\partial\sigma_w^2/\partial z = 0$ (roughly delineated by the vertical dashed line in Figure 8). Interestingly, the work here suggests that within the ISL where $\partial\sigma_w^2/\partial z = 0$, down-gradient models fail to predict a finite $\overline{w'^3}$ and a rectification based on $\overline{w'q'}$ is required in this zone. For this reason, the gradient-diffusion representation linking $\overline{w'q'}$ to $\partial K/\partial z$ in equation 45 is explored in Figure 9. Note that for $z/\delta < 0.1$, data are shaded because these points are near or within the sublayer below the ISL for many of the data sets, and are in the near-wall region where there is greater uncertainty due to experimental constraints such as measurement resolution. In this analysis, q' is not measured but estimated as $q' = 2u'^2$. By and large and for $0.08 < z/\delta < 0.8$, the gradient-diffusion representation with a diffusivity based on $\kappa z u_* \phi_L(z)$ predicts well the vertical transport of energy needed to describe Sk_w. It can be stated that the down-gradient model for $\overline{w'q'}$ captures the essential mechanisms needed to describe Sk_w in equation 46 and will be used later on to demonstrate that Sk_w is dominated by this term. Returning to equation 46, there are two second-order velocity gradients that impact Sk_w. Since the gradients are measured and the diffusivities are modeled but expected to be comparable based on the choice of τ_s, the significance of the gradients, normalized by z and u_*, are first discussed in Figure 10. From this Figure, it is clear that when $z/\delta > 0.1$, the normalized $\partial\sigma_u^2/\partial z$ are some 4-5 times larger in magnitude than $\partial\sigma_w^2/\partial z$. Within the ISL, $\partial\sigma_w^2/\partial z \approx 0$ and much of the finite Sk_w in the ISL is associated with $\partial\sigma_u^2/\partial z$ (as predicted by the prognostic approach). Hence, it is conjectured that for $0.1 < z/\delta < 1$, the dominant term on the vertical velocity skewness is not related to $\partial\sigma_w^2/\partial z$. That is, the vertical velocity skewness is primarily driven by

$$Sk_{w,t} = -\frac{2}{3}\left(1 - \frac{2c_2}{C_R}\right)\frac{\kappa z u_* \phi_L(z)}{\sigma_w^3}\frac{\partial(\sigma_u^2)}{\partial z}. \qquad (48)$$

This conjecture is directly tested in Figure 11, which compares measured Sk_w with predictions from equation 48 $Sk_{w,t}$ in the range of $0.1 < z/\delta < 1$ (measured σ_u^2 and σ_w^3 are used in these calculations). The agreement is quite acceptable given the uncertainty in assumed $\phi_L(z)$ and measured longitudinal velocity variance gradients. This finding explains why equation 4 fails when not accounting for the large-scale adjustment, which is modeled here using equation 48. An implication of including ϕ_L is that in the outer layer, eddies commensurate to δ and inner layer eddies commensurate to z are significant. To what degree the contribution of these eddies is evident in the experiments here is now considered using a data set where the sampling duration enables statistical convergence at the very large scales.

D. Further analysis: Co-spectral results

The co-spectrum between w' and $w'^2 - \overline{w'^2}$ is analyzed and a typical shape is shown in Figure 12 for the longest sam-

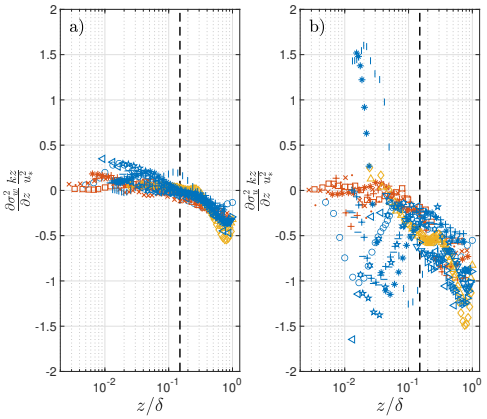

FIG. 10. Normalized (a) vertical and (b) horizontal velocity gradients as a function of the normalized wall normal distance z/δ. The vertical dashed lines roughly indicate the upper limit of the ISL.

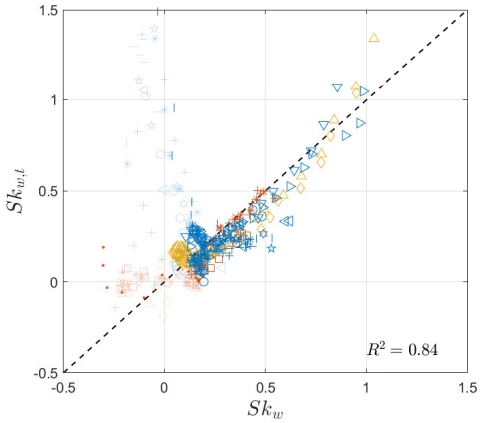

FIG. 11. Comparison between measured Sk_w and predictions from equation 48 with $C_R = 1.8$, $c_2 = 0.1$, u_*, and the gradients reported in Figure 10. The shaded markers indicate $z/\delta < 0.1$. The one-to-one line is also shown.

pling duration data set needed to resolve large and very large structures (i.e. MNS in Table I). Consistent with expectations from equation 47, when $z/\delta > 0.2$, scales defined by both z and δ play a role as anticipated from an eddy diffusivity that scales with $z(1-z/\delta)$. At $k\delta = 0.9$ the dominant length scale is δ because z and δ are comparable. Likewise, in the region where $z/\delta < 0.1$, attached eddies ($kz = 0.4$) appear to contribute most to the co-spectral content of w' and $w'^2 - \sigma_w^2$, as expected, because z/δ no longer contributes to the eddy diffusivity. These findings independently support the formulation in equation 47 that identifies z and δ (through ϕ_L) as the limiting scales to be accommodated in models for Sk_w for the ISL and outer layer region. However, caution should be exercised in such naive binary representation of length scales as the analysis also shows that eddies up to 10δ (often related to very large scale motion or VLSM) still have finite contributions on the co-spectra.

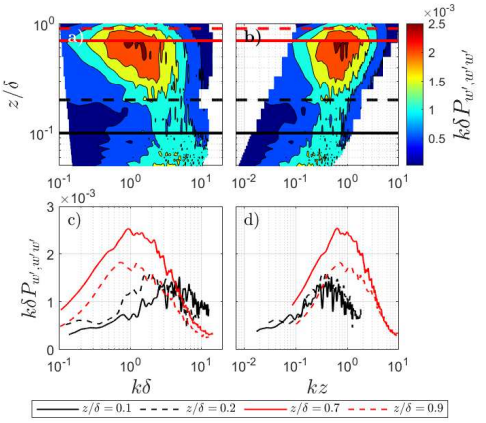

FIG. 12. The measured co-spectra of w'/σ_w and $(w'^2/\sigma_w^2) - 1$ as a function of normalized wavenumber and height (z/δ). The wavenumber k is normalized with δ in the left panels (a, c) and with z in the right panels (b, d). The bottom panels (c,d) report the co-spectra at 4 heights: $z/\delta = 0.1$ in the ISL, $z/\delta = 0.2$ transitioning from the ISL to the outer layer, $z/\delta = 0.7$ in the outer layer, and $z/\delta = 0.9$ near the top of the boundary layer. Those locations are also shown in the top panels as dashed horizontal lines. The 95 confidence bound for the co-spectra is approximately 0.84 to 1.16 times $k\delta P_{w',w'w'}$.

V. CONCLUSIONS

The present work explores the vertical velocity skewness (Sk_w) in wall bounded flows covering smooth, rough, and permeable surfaces across a wide range of Reynolds numbers ($Re_\tau = 331 - 13683$). The exploration focused on diagnostic and prognostic models for Sk_w. The following conclusions can be drawn:

- For the diagnostic models, it was shown that third order cumulant expansions for the single and joint (with u') PDFs establish links between duration of updrafts Γ_+, the relative importance of ejections over sweeps to momentum transport ΔS_0, and Sk_w. Those derivations are statistical in nature and only offer constraints on the vertical velocity skewness values. However, they make no contact with the Navier-Stokes equations or the physics of turbulence.

- The fractional area/mass flux approach that is routinely used in convective boundary layer models to correct gradient-diffusion formulations was also explored (for near-neutral conditions) across many roughness values and Reynolds numbers. This approach was used to invert for the fractional area of updrafts ($= a$) to match Γ_+. The findings support a constant a independent of z in the range $0.1 < z/\delta < 0.3$. When combined with third order cumulant expansion, a unique link between a and Γ_+ was established. It was also shown that such a model predicts a relation between the vertical velocity flatness factor FF_w and Sk_w given by $FF_w = \alpha_1(Sk_w^2 + 1)$ with $\alpha_1 = 1$ independent of a. Such $\alpha_1 = 1$ is the minimum required to satisfy the realizability constraints. The data here were used to examine α_1 as a function of z/δ and it was shown $\alpha_1 = 3.3$ is plausible for $0.1 < z/\delta < 1$. Such a value is sufficiently close to the value predicted from a quasi-Gaussian approximation ($\alpha_1 = 3$).

- The prognostic approach considered the budgets for $\overline{w'}$, $\overline{w'^2}$, and $\overline{w'^3}$. It was shown that the budget of $\overline{w'}$ yields a constant σ_w^2 independent of z/δ only when the mean pressure is hydrostatic. This finding establishes a link between the emergence of a constant σ_w^2 with respect to z expected in the ISL and models for the mean pressure.

- The budgets for $\overline{w'^2}$ and $\overline{w'^3}$, when combined together, resulted in a model for $\overline{w'^3}$ that has two contributions: a gradient diffusion contribution arising from inertia that links $\overline{w'^3}$ to $\partial\sigma_w^2/\partial z$ and a non-local contribution that links $\overline{w'^3}$ to the turbulent transport of kinetic energy $\overline{w'q'}$. This transport term arises from return-to-isotropy considerations originally established when closing the $\overline{w'^2}$ budget using a linear Rotta scheme.

- The term $\overline{w'q'}$ was shown to be reasonably approximated with a down gradient model with respect to turbulent kinetic energy K provided the standard eddy diffusivity $\kappa z u_*$ is multiplied by a correction function for outer layer eddies $\phi_L(z/\delta)$. The contribution from $\overline{w'q'}$ explains much of the Sk_w values in the range of $0.1 < z/\delta < 1$ when using $\kappa z u_* \phi_L$ and $\partial K/\partial z$. This finding offers a bridge to the diagnostic structural models that already demonstrated $\overline{w'q'} = -(3/4)\Delta S_o(A_{SM}\sigma_u^2\sigma_w + B_{SM}\sigma_w^3)$, where $A_{SM} = 1.34$ and $B_{SM} = 1.59$ are constants[9,10]. Thus, the vertical velocity skewness can now be written as

$$Sk_w = \overbrace{-\frac{2}{3C_R}\frac{\tau_s}{\sigma_w}\frac{\partial\overline{w'w'}}{\partial z}}^{\text{local effects}} + \underbrace{\beta_L\frac{3}{4}\Delta S_o\left(A_{SM}\frac{\sigma_u^2}{\sigma_w^2} + B_{SM}\right)}_{\text{large scale adjustment}}. \tag{49}$$

  When ejections dominate momentum transport over sweeps, $\Delta S_o < 0$ and Sk_w remains positive even when $\partial\sigma_w^2/\partial z = 0$ (i.e. negligible local effects, mean pressure is hydrostatic). This result can also be expressed as a mass flux model given the relation between ΔS_o and Γ_+ in Figure 6, and the relation between Γ_+ and the fractional area in the mass flux approach. This superposition of down-gradient and mass flux approaches is widely used in turbulence parameterization in climate models. Thus, the work here offers a new perspective of how to combine local and non-local effects when modeling Sk_w and shows the interconnection between diagnostic and prognostic models.

- In canonical wall-bounded flows, large and very large scale semi-organized turbulent structures that exceed in size the boundary layer depth δ contribute significantly to turbulent kinetic energy[68,70,74,75] and other higher order flow statistics for u' even in the ISL[69,76]. To what degree these structures impact $\overline{w'^3}$ has not been resolved from earlier studies. The work here demonstrates that such structures still have a finite contribution to the asymmetry in w'. To what degree their effects can be accommodated through the proposed outer layer correction ϕ_L to the eddy diffusivity $\kappa z u_*$ requites further exploration.

- Diagnostic and prognostic models exhibit remarkable consistency in both the ISL and outer layer, regardless of the underlying surface and Reynolds numbers. This suggests that the effects of roughness and Reynolds numbers are confined to the roughness sublayer itself along with its thickness (deepest in terms of z/δ for the lowest Re_τ=331). However, the uncertainties in measurements within the near-wall region, do not allow speculate claims on surface type effects below ISL. Furthermore, the findings show no significant dependence on the Reynolds number within the range of R_τ from 8×10^2 to 1×10^5. The consistency of the results, despite variations in Re_τ and surface type, suggests the universality of Sk_w above the roughness sublayer or buffer layer.

To summarize, the breadth of the results presented here provides an enhanced understanding of vertical velocity skewness that spans the flow phenomenology, governing Navier-Stokes equations, and statistical outcomes of turbulence. The asymmetry is linked to large-scale coherent turbulent structures (Figure 12), which in a simplified sense includes sweeps ad ejections. A model for skewness must therefore include a non-local adjustment to account for these large-scale eddies (equation 6). The form of the adjustment can be determined prognostically from the governing budget equations (equation 44) or diagnostically from statistics that quantify properties of the turbulent structures (e.g. ΔS_o and Γ_+). Regardless of the approach, the non-local adjustment is well described by the kinetic energy transport $\overline{w'q'}$ (Figure 11) as shown here.

In the second and third moment prognostic models, the following assumptions have been made: (i) the linear return-to-isotropy (Rotta) model, and (ii) isotropy of the dissipation rate to model pressure-velocity interactions and viscous de-

struction. The Rotta model, which neglects nonlinear interactions, particularly underperforms in the near-wall region, where anisotropy is sustained by the mean strain rate. This limitation may be overcome by adopting well known nonlinear return to isotropy models[61,77–80]. The assumption of isotropy in the dissipation rate implies that isotropy is well-established at the dissipation scales (i.e., small or microscale). While this assumption is reasonably valid at moderate-to-high Reynolds numbers, it can be problematic at low Reynolds numbers, where anisotropy persists even at the dissipation scale.

While these results do not address all aspects of ABL parameterizations needed in models such as CLUBB, they do offer bench-mark outcomes for the adiabatic limit based on controlled laboratory experiments. In this respect, they may be viewed as necessary but not sufficient to progress on turbulence parameterizations for the asymmetry in w' within climate models. The LES framework may benefit from the Sk_w models here as LES is repeatedly called upon to contrast the effects of ground inhomogeneities on cloud formation when referenced to homogeneous cases. As already discussed, Sk_w is expected to be smaller for heterogeneous ground cover given the disproportionate impact of heterogeneity on σ_w^2 when compared to $\overline{w'^3}$. Thus, bench-mark expectations for the Sk_w profiles of what the homogeneous cover case ought to be for a set of surface roughness and Reynolds number runs within the LES is, undoubtedly, necessary.

Future effort will bifurcate in two directions. One seeks to explore the extension of these approaches (prognostic and diagnostic) to stratified flows in the atmosphere (mainly surface layer and roughness sublayer including vegetated and urban employing atmospheric data) - where buoyancy, elevated Reynolds numbers, Coriolis forces, and enhanced roughness values are expected. The other seeks dedicated open channel flow experiments that will clarify the contribution of the many eddy sizes, including large-scale structures, on the co-spectra of w'- w'^2, w' - u'^2, and w'-w'^3. These co-spectra (and concomitant co-spectral peak similarities) can assist in the formulation of future prognostic models or revisions to a linear $\phi_L(z) = 1 - z/\delta$. These future experiments do require extended sampling duration to reliably resolve contributions of very large eddy sizes.

ACKNOWLEDGMENTS

EB acknowledges Politechnico di Torino (Italy) for supporting the visit to Duke University. GK acknowledges support from the U.S. National Science Foundation (NSF-AGS-2028633) and the U.S. Department of Energy (DE-SC0022072). DP acknowledges support from Fondo europeo di sviluppo regionale (FESR) for project Bacini Ecologicamente sostenibili e sicuri, concepiti per l'adattamento ai Cambiamenti ClimAtici (BECCA) in the context of Alpi Latine COoperazione TRAnsfrontaliera (ALCOTRA) and project Nord Ovest Digitale e Sostenibile - Digital innovation toward sustainable mountain (Nodes - 4). DV and CM acknowledge European Union's Horizon 2020 research and innovation programme under the Marie Sklodowska-Curie grant agreement No 101022685 (SHIEELD).

CONFLICT OF INTEREST STATEMENT

The Authors have no conflicts to disclose.

DATA AVAILABILITY STATEMENT

The data that support the findings of this study are available from the corresponding author upon reasonable request.

[1] J. P. Peixóto and A. H. Oort, "Physics of climate," Reviews of Modern Physics **56**, 365 (1984).
[2] K. E. Trenberth, *Climate System Modeling* (Cambridge University Press, 1992).
[3] K. R. Sreenivasan, "Fluid turbulence," Reviews of Modern Physics **71**, S383 (1999).
[4] K. Hasselmann, "Stochastic climate model. part i: Theory," Tellus **28**, 289–305 (1976).
[5] R. B. Stull, *An Introduction to Boundary Layer Meteorology*, Vol. 13 (Springer Science & Business Media, 1988).
[6] J. D. Fuentes, M. Chamecki, R. M. N. Dos Santos, C. Von Randow, P. C. Stoy, G. Katul, D. Fitzjarrald, A. Manzi, T. Gerken, A. Trowbridge, *et al.*, "Linking meteorology, turbulence, and air chemistry in the Amazon rain forest," Bulletin of the American Meteorological Society **97**, 2329–2342 (2016).
[7] J. C. Wyngaard, *Turbulence in the Atmosphere* (Cambridge University Press, 2010).
[8] H. Nakagawa and I. Nezu, "Prediction of the contributions to the Reynolds stress from bursting events in open-channel flows," Journal of Fluid Mechanics **80**, 99–128 (1977).
[9] M. Raupach, "Conditional statistics of Reynolds stress in rough-wall and smooth-wall turbulent boundary layers," Journal of Fluid Mechanics **108**, 363–382 (1981).
[10] M. Heisel, G. G. Katul, M. Chamecki, and M. Guala, "Velocity asymmetry and turbulent transport closure in smooth-and rough-wall boundary layers," Physical Review Fluids **5**, 104605 (2020).
[11] H. Fernholz and P. Finleyt, "The incompressible zero-pressure-gradient turbulent boundary layer: an assessment of the data," Progress in Aerospace Sciences **32**, 245–311 (1996).
[12] D. Poggi, A. Porporato, L. Ridolfi, J. Albertson, and G. Katul, "The effect of vegetation density on canopy sub-layer turbulence," Boundary-Layer Meteorology **111**, 565–587 (2004).
[13] R. H. Shaw and I. Seginer, "Calculation of velocity skewness in real and artificial plant canopies," Boundary-Layer Meteorology **39**, 315–332 (1987).
[14] A. Maurizi, "On the dependence of third-and fourth-order moments on stability in the turbulent boundary layer," Nonlinear Processes in Geophysics **13**, 119–123 (2006).
[15] A. S. Monin and A. M. Obukhov, "Basic laws of turbulent mixing in the surface layer of the atmosphere," Contrib. Geophys. Inst. Acad. Sci. USSR **151**, e187 (1954).
[16] O. Chiba, "Stability dependence of the vertical wind velocity skewness in the atmospheric surface layer," Journal of the Meteorological Society of Japan. Ser. II **56**, 140–142 (1978).
[17] J. Wyngaard and O. Coté, "The budgets of turbulent kinetic energy and temperature variance in the atmospheric surface layer," Journal of the Atmospheric Sciences **28**, 190–201 (1971).
[18] M. A. LeMone, "Some observations of vertical velocity skewness in the convective planetary boundary layer," Journal of the Atmospheric Sciences **47**, 1163–1169 (1990).
[19] D. H. Lenschow, M. Lothon, S. D. Mayor, P. P. Sullivan, and G. Canut, "A comparison of higher-order vertical velocity moments in the convective boundary layer from lidar with in situ measurements and large-eddy simulation," Boundary-Layer Meteorology **143**, 107–123 (2012).

[20]K. Ghannam, T. Duman, S. T. Salesky, M. Chamecki, and G. Katul, "The non-local character of turbulence asymmetry in the convective atmospheric boundary layer," Quarterly Journal of the Royal Meteorological Society **143**, 494–507 (2017).
[21]K. Barskov, D. Chechin, I. Drozd, A. Artamonov, A. Pashkin, A. Gavrikov, M. Varentsov, V. Stepanenko, and I. Repina, "Relationships between second and third moments in the surface layer under different stratification over grassland and urban landscapes," Boundary-Layer Meteorology **187**, 311–338 (2023).
[22]J. H. Bærentsen and R. Berkowicz, "Monte Carlo simulation of plume dispersion in the convective boundary layer," Atmospheric Environment (1967) **18**, 701–712 (1984).
[23]A. K. Luhar and R. E. Britter, "A random walk model for dispersion in inhomogeneous turbulence in a convective boundary layer," Atmospheric Environment **23**, 1911–1924 (1989).
[24]J. C. Wyngaard and J. C. Weil, "Transport asymmetry in skewed turbulence," Physics of Fluids A: Fluid Dynamics **3**, 155–162 (1991).
[25]A. Maurizi and F. Tampieri, "Velocity probability density functions in Lagrangian dispersion models for inhomogeneous turbulence," Atmospheric Environment **33**, 281–289 (1999).
[26]P. P. Sullivan and E. G. Patton, "The effect of mesh resolution on convective boundary layer statistics and structures generated by Large-Eddy Simulation," Journal of the Atmospheric Sciences **68**, 2395–2415 (2011).
[27]C.-H. Moeng and R. Rotunno, "Vertical-velocity skewness in the buoyancy-driven boundary layer," Journal of the Atmospheric Sciences **47**, 1149–1162 (1990).
[28]F. Quintarelli, "A study of vertical velocity distributions in the planetary boundary layer," Boundary-Layer Meteorology **52**, 209–219 (1990).
[29]S. Zilitinkevich, V. M. Gryanik, V. Lykossov, and D. Mironov, "Third-order transport and nonlocal turbulence closures for convective boundary layers," Journal of the Atmospheric Sciences **56**, 3463–3477 (1999).
[30]M. Huang, H. Xiao, M. Wang, and J. D. Fast, "Assessing CLUBB PDF closure assumptions for a continental shallow-to-deep convective transition case over multiple spatial scales," Journal of Advances in Modeling Earth Systems **12**, e2020MS002145 (2020).
[31]P. Bogenschutz, A. Gettelman, H. Morrison, V. Larson, D. Schanen, N. Meyer, and C. Craig, "Unified parameterization of the planetary boundary layer and shallow convection with a higher-order turbulence closure in the community atmosphere model: Single-column experiments," Geoscientific Model Development **5**, 1407–1423 (2012).
[32]G. L. Mellor and T. Yamada, "Development of a turbulence closure model for geophysical fluid problems," Reviews of Geophysics **20**, 851–875 (1982).
[33]T. Li, M. Wang, Z. Guo, B. Yang, Y. Xu, X. Han, and J. Sun, "An updated CLUBB PDF closure scheme to improve low cloud simulation in CAM6," Journal of Advances in Modeling Earth Systems **14**, e2022MS003127 (2022).
[34]T. Waterman, A. D. Bragg, G. Katul, and N. Chaney, "Examining parameterizations of potential temperature variance across varied landscapes for use in earth system models," Journal of Geophysical Research: Atmospheres **127**, e2021JD036236 (2022).
[35]P. J. Mason, "Large-eddy simulation of the convective atmospheric boundary layer," Journal of the Atmospheric Sciences **46**, 1492–1516 (1989).
[36]J. André, G. De Moor, P. Lacarrere, and R. Du Vachat, "Turbulence approximation for inhomogeneous flows: Part I. the clipping approximation," Journal of the Atmospheric Sciences **33**, 476–481 (1976).
[37]M. Millionshchikov, "On the theory of homogeneous isotropic turbulence," in *Dokl. Akad. Nauk SSSR*, Vol. 32 (1941) pp. 611–614.
[38]B. E. Launder, G. J. Reece, and W. Rodi, "Progress in the development of a Reynolds-stress turbulence closure," Journal of Fluid Mechanics **68**, 537–566 (1975).
[39]J. L. Lumley, "Computational modeling of turbulent flows," Advances in Applied Mechanics **18**, 123–176 (1979).
[40]K. Hanjalic, "One-point closure models for buoyancy-driven turbulent flows," Annual Review of Fluid Mechanics **34**, 321–347 (2002).
[41]S. Corrsin, "Limitations of gradient transport models in random walks and in turbulence," in *Advances in Geophysics*, Vol. 18 (Elsevier, 1975) pp. 25–60.
[42]G. Katul and J. D. Albertson, "An investigation of higher-order closure models for a forested canopy," Boundary-Layer Meteorology **89**, 47–74 (1998).
[43]D. Poggi, G. Katul, and J. Albertson, "Momentum transfer and turbulent kinetic energy budgets within a dense model canopy," Boundary-Layer Meteorology **111**, 589–614 (2004).
[44]K. Abdella and A. Petersen, "Third-order moment closure through a mass-flux approach," Boundary-Layer Meteorology **95**, 303–318 (2000).
[45]J. Deardorff, "Theoretical expression for the countergradient vertical heat flux," Journal of Geophysical Research **77**, 5900–5904 (1972).
[46]V. Canuto, F. Minotti, C. Ronchi, R. Ypma, and O. Zeman, "Second-order closure PBL model with new third-order moments: Comparison with LES data," Journal of the Atmospheric Sciences **51**, 1605–1618 (1994).
[47]Y. Nagano and M. Tagawa, "Statistical characteristics of wall turbulence with a passive scalar," Journal of Fluid Mechanics **196**, 157–185 (1988).
[48]Y. Nagano and M. Tagawa, "A structural turbulence model for triple products of velocity and scalar," Journal of Fluid Mechanics **215**, 639–657 (1990).
[49]S. M. Ölçmen, R. L. Simpson, and J. W. Newby, "Octant analysis based structural relations for three-dimensional turbulent boundary layers," Physics of Fluids **18** (2006).
[50]D. Cava, G. Katul, A. Scrimieri, D. Poggi, A. Cescatti, and U. Giostra, "Buoyancy and the sensible heat flux budget within dense canopies," Boundary-Layer Meteorology **118**, 217–240 (2006).
[51]D. Poggi and G. Katul, "Flume experiments on intermittency and zero-crossing properties of canopy turbulence," Physics of Fluids **21**, 065103 (2009).
[52]G. Katul, C.-I. Hsieh, G. Kuhn, D. Ellsworth, and D. Nie, "Turbulent eddy motion at the forest-atmosphere interface," Journal of Geophysical Research: Atmospheres **102**, 13409–13421 (1997).
[53]D. Cava, G. G. Katul, A. Molini, and C. Elefante, "The role of surface characteristics on intermittency and zero-crossing properties of atmospheric turbulence," Journal of Geophysical Research: Atmospheres **117** (2012).
[54]G. Katul, O. Peltola, T. Grönholm, S. Launiainen, I. Mammarella, and T. Vesala, "Ejective and sweeping motions above a peatland and their role in relaxed-eddy-accumulation measurements and turbulent transport modelling," Boundary-Layer Meteorology **169**, 163–184 (2018).
[55]S. Alberghi, A. Maurizi, and F. Tampieri, "Relationship between the vertical velocity skewness and kurtosis observed during sea-breeze convection," Journal of Applied Meteorology **41**, 885 – 889 (2002).
[56]J. Rotta, "Statistische Theorie nichthomogener Turbulenz," Zeitschrift für Physik **129**, 547–572 (1951).
[57]E. Bou-Zeid, X. Gao, C. Ansorge, and G. G. Katul, "On the role of return to isotropy in wall-bounded turbulent flows with buoyancy," Journal of Fluid Mechanics **856**, 61–78 (2018).
[58]H.-B. Su and Paw U, Kyaw Tha, "Large-eddy simulation of Reynolds stress budgets in and above forests in neutral atmospheric boundary layers," Boundary-Layer Meteorology **187**, 457–500 (2023).
[59]K. Hanjalić and B. Launder, "Reassessment of modeling turbulence via Reynolds averaging: A review of second-moment transport strategy," Physics of Fluids **33** (2021).
[60]S. B. Pope, *Turbulent Flows* (Cambridge University Press, Cambridge, UK, 2000).
[61]I. Stiperski, G. G. Katul, and M. Calaf, "Universal return to isotropy of inhomogeneous atmospheric boundary layer turbulence," Physical Review Letters **126**, 194501 (2021).
[62]P. R. Spalart, "Direct simulation of a turbulent boundary layer up to R_θ= 1410," Journal of Fluid Mechanics **187**, 61–98 (1988).
[63]O. Zeman and J. L. Lumley, "Modeling buoyancy driven mixed layers," Journal of the Atmospheric Sciences **33**, 1974–1988 (1976).
[64]E. Buono, G. Katul, M. Heisel, D. Vettori, D. Poggi, C. Peruzzi, and C. Manes, "The vertical-velocity skewness in the inertial sublayer of turbulent wall flows," Journal of Fluid Mechanics (in press) (2024).
[65]F. Lopez and M. H. García, "Wall similarity in turbulent open-channel flow," Journal of Engineering Mechanics **125**, 789–796 (1999).
[66]A. K. Blackadar, "The vertical distribution of wind and turbulent exchange in a neutral atmosphere," Journal of Geophysical Research **67**, 3095–3102 (1962).
[67]J. J. O'Brien, "A note on the vertical structure of the eddy exchange coefficient in the planetary boundary layer," Journal of the Atmospheric Sciences **27**, 1213–1215 (1970).

[68]T. Banerjee and G. G. Katul, "Logarithmic scaling in the longitudinal velocity variance explained by a spectral budget," Physiscs of Fluids **25**, 125106 (2013).
[69]I. Marusic, J. P. Monty, M. Hultmark, and A. J. Smits, "On the logarithmic region in wall turbulence," Journal of Fluid Mechanics **716**, R3 (2013).
[70]A. Townsend, *The Structure of Turbulent shear flow* (Cambridge University Press, 1976).
[71]C. Manes, D. Poggi, and L. Ridolfi, "Turbulent boundary layers over permeable walls: scaling and near-wall structure," Journal of Fluid Mechanics **687**, 141–170 (2011).
[72]C. Peruzzi, D. Poggi, L. Ridolfi, and C. Manes, "On the scaling of large-scale structures in smooth-bed turbulent open-channel flows," Journal of Fluid Mechanics **889**, A1 (2020).
[73]D. Poggi, A. Porporato, and L. Ridolfi, "An experimental contribution to near-wall measurements by means of a special laser doppler anemometry technique," Experiments in Fluids **32**, 366–375 (2002).
[74]I. Marusic and G. J. Kunkel, "Streamwise turbulence intensity formulation for flat-plate boundary layers," Physics of Fluids **15**, 2461–2464 (2003).
[75]G. Katul, "The anatomy of large-scale motion in atmospheric boundary layers," Journal of Fluid Mechanics **858**, 1–4 (2019).
[76]K. Y. Huang and G. G. Katul, "Profiles of high-order moments of longitudinal velocity explained by the random sweeping decorrelation hypothesis," Physical Review Fluids **7**, 044603 (2022).
[77]S. Sarkar and C. G. Speziale, "A simple nonlinear model for the return to isotropy in turbulence," Physics of Fluids A: Fluid Dynamics **2**, 84–93 (1990).
[78]M. K. Chung and S. K. Kim, "A nonlinear return-to-isotropy model with Reynolds number and anisotropy dependency," Physics of Fluids **7**, 1425–1437 (1995).
[79]K.-S. Choi and J. L. Lumley, "The return to isotropy of homogeneous turbulence," Journal of Fluid Mechanics **436**, 59–84 (2001).
[80]H. Warrior, S. Mathews, S. Maity, and K. Sasmal, "An improved model for the return to isotropy of homogeneous turbulence," Journal of Fluids Engineering **136**, 034501 (2014).